HHS Public Access

Author manuscript

Mol Imaging Biol. Author manuscript; available in PMC 2015 May 13.

Published in final edited form as:

Mol Imaging Biol. 2013 April ; 15(2): 166–174. doi:10.1007/s11307-012-0585-8.

Tumor-Specific Targeting With Modified Sindbis Viral Vectors: Evaluation with Optical Imaging and Positron Emission Tomography *In Vivo*

Lars Stelter[1,2], **Jen-Chieh Tseng**[3], **Armen Torosjan**[1], **Brandi Levin**[3], **Valerie A. Longo**[1], **Nagavarakishore Pillarsetty**[1], **Pat Zanzonico**[1], **Daniel Meruelo**[3], and **Steven M. Daniel**[1,4,5]

[1]Nuclear Medicine Service, Department of Radiology, Memorial Sloan-Kettering Cancer Center, New York, USA

[2]Department of Radiology, Charité–Universitätsmedizin Berlin, Berlin, Germany

[3]NYU Cancer Institute and the NYU GeneTherapy Center, Department of Pathology, NYU School of Medicine, New York University, New York, USA

[4]Ludwig Institute for Cancer Research, Memorial Sloan-Kettering Cancer Center, New York, USA

[5]Program in Molecular Pharmacology and Chemistry, Memorial Sloan-Kettering Cancer Center, New York, USA

Abstract

Purpose—Sindbis virus (SINV) infect tumor cells specifically and systemically throughout the body. Sindbis vectors are capable of expressing high levels of transduced suicide genes and thus efficiently produce enzymes for prodrug conversion in infected tumor cells. The ability to monitor suicide gene expression levels and viral load in patients, after administration of the vectors, would significantly enhance this tumor-specific therapeutic option.

Procedures—The tumor specificity of SINV is mediated by the 67-kDa laminin receptor (LR). We probed different cancer cell lines for their LR expression and, to determine the specific role of LR-expression in the infection cycle, used different molecular imaging strategies, such as bioluminescence, fluorescence molecular tomography, and positron emission tomography, to evaluate SINV-mediated infection *in vitro* and *in vivo*.

Results—All cancer cell lines showed a marked expression of LR. The infection rates of the SINV particles, however, differed significantly among the cell lines.

Conclusion—We used novel molecular imaging techniques to visualize vector delivery to different neoplatic cells. SINV infection rates proofed to be not solely dependent on cellular LR expression. Further studies need to evaluate the herein discussed ways of cellular infection and viral replication.

Correspondence to: Lars Stelter; lars.stelter@charite.de.

Conflict of Interest. The contents of this study are being used for a patent. According to the rules and regulations of New York University School of Medicine, if this patent is licensed by a third party, some of the authors (JT, BL, and DM) may receive benefits in the form of royalties or equity participation. All other authors declare that they have no conflict of interest.

Keywords

Molecular imaging; Sindbis virus; Tumor targeting; Bioluminescence; FMT; PET

Introduction

Viral vectors based on the Sindbis virus (SINV), a blood-borne alphavirus, infect xenograft tumor cells specifically and systemically in preclinical mouse models [1, 2]. The tumor specificity of Sindbis vectors is mediated by the 67-kDa high-affinity laminin receptor (LR) [3], which is overexpressed in multiple types of human tumors [4–7]. An important characteristic of Sindbis vectors for cancer therapy is that the native virus itself can induce apoptosis in neoplastic mammalian cells while being nontoxic to nontarget tissues [8–10]. Furthermore, Sindbis vectors are capable of expressing high levels of transduced suicide genes and thus efficiently produce enzymes for prodrug conversion in infected tumor cells making them applicable for gene-directed enzyme-prodrug therapy (GDEPT). One of the best-studied enzyme/prodrug systems for cancer GDEPT is the herpes simplex virus thymidine kinase type 1/ganciclovir (HSV1-tk/GCV) system [11]. It is highly effective in eradicating rapidly dividing tumor cells by inhibiting their DNA polymerase while sparing nonproliferating normal tissues [12–14]. The ability to monitor the levels of suicide gene expression in tumors after administering the vectors would significantly improve GDEPT. Positron emission tomography (PET) tracers such as [^{124}I]-2′-fluoro-2′-deoxy-1-β-$_{D}$-arabinofuranosyl-5-iodo-uracil ([^{124}I]-FIAU) and [^{18}F]-2′-fluoro-2′-deoxy-1-β-$_{D}$-β-arabinofuranosyl-5-ethyluracil ([^{18}F]-FEAU), which act as thymidine analogs, have already been developed for monitoring HSV1-tk activity in living subjects [15, 16].

The aims of this study included the determination and optimization of Sindbis virus-mediated infection of different human tumor cells, *in vitro* and *in vivo*, and evaluation of the specific role of laminin receptor expression levels in the infection process. In a proof-of-principle approach, optical imaging modalities (bioluminescence and fluorescence) and PET were utilized to visualize and quantitate these processes and their therapeutic effects.

Material and Methods

Cell Lines and Vector Production

All cell lines were obtained from the American Type Culture Collection (Manassas, VA, USA). BHK fibroblast cells were maintained in minimum essential alpha-modified media with 5 % fetal bovine serum (FBS). Colon carcinoma cells HT29 were cultured in McCoy's 5A medium supplemented with 10 % FBS. The melanoma cell lines SK-MEL 10 and SK-MEL 28 as well as HeLa (cervical cancer), DU145 (prostatic cancer), and H1650 (non-small-cell lung cancer) cells were kept in minimal essential media with 10%FBS. All basal media were supplemented with 100 μg/ml of penicillin–streptomycin and 0.5 μg/ml of amphotericin b. Replication-deficient Sindbis vectors were produced by electroporation of both replicon RNA (SinRep5) and helper RNA (DH-BB) into BHK cells as previously described [1]. The HSV-1 thymidine kinase gene was excised from the pORF-HSV1tk plasmid and inserted into the *Pml*I site of the SinRep5 plasmid for Sindbis/tk vector

production. Sindbis/firefly luciferase gene (FLuc) vectors were produced using a DNA fragment containing the FLuc from the *Nhe*I and *Xba*I sites of the plasmid pGL3 and subcloned into the *Xba*I site of the SinRep plasmid to construct the SinRep/FLuc vector [1]. For designing a replication-competent (RC) Sindbis vector carrying also the firefly luciferase gene as reporter, a DNA segment containing a subgenomic promoter and Sindbis viral structural genes were excised from the ptRNA-DHBB plasmid using *NsiI* and *BamHI* enzymes and then inserted into pSinRep5/Fluc at the StuI site; vectors were also prepared using the *in vitro* transcription/electroporation method.

Western Blots

Cells were washed with ice-cold phosphate-buffered saline (PBS) and lysed with RIPA buffer. The lysates were centrifuged, the supernatant added to LDS sample buffer and the sample heated at 90 °C for 10 min. The protein concentration was determined using the Bradford assay and a 50 μg protein sample added to a sodium dodecyl sulfate polyacrylamide gel electrophoresis gel well. The gel ran at 120 V for ~120 min. Proteins were transferred onto a NC membrane at 80 mA for 1 h. The membrane was blocked with blocking buffer and treated with a 1:1,000 dilution of the rabbit polyclonal to 37 kDa laminin receptor (H-141, Santa Cruz Biotechnology, Santa Cruz, CA, USA) for 12 h at 4 °C. After a washing step, the membrane was incubated with a 1:5,000 dilution of horseradish peroxidise-conjugated goat anti-rabbit IgG for 1 h at room temperature. After a final washing step, the membrane was treated with detection reagents and exposed to film.

Sindbis/FLuc Uptake In Vitro

To determine the infectivity of the Sindbis viral vector in different cell lines, a dilution series of Sindbis/FLuc viral vector particles (1:1, $1:1 \times 10^1$, $1:1 \times 10^2$, $1:1 \times 10^3$, $1:1 \times 10^4$; undiluted particles equal ~100 colony forming units (CFU) in 300 μL Opti-MEM medium) were incubated at 37 °C for 1 h with 2×10^5 each of BHK, SK-MEL 10, SK-MEL 28, HT29, HeLa, DU145, or H1650 cells that were previously cultured in 12-well plates. After incubation, the infection medium was replaced with regular culture medium and the cells were incubated overnight at 37 °C. The next day, cells were assayed by the Steady-Glo® Luciferase Assay System (Promega Corp., Madison, WI, USA). For each cell line, three independent experiments were performed. For each experiment, control cells were mock-infected with 300 μL of normal culture medium and incubated at 37 °C for 1 h.

Bioluminescence Imaging (IVIS 200)

All animal experiments were performed in accordance with the National Institute of Health and MSKCC Institutional Animal Care and Use Committee guidelines. C.B-17-SCID mice (Charles River, Kingston, NY, USA; female, 6–8 weeks old) were injected subcutaneously with 4×10^6 BHK and/or SK-MEL 10 cells in 0.2 mL culture medium/Matrigel™ (BD Biosciences, Bedford, MA, USA) in the shoulder region on day 0.We choose a combined tumor model, having BHK and SK-MEL 10 tumors inoculated side by side, and a single tumor model, just SK-MEL 10 inoculation, and randomly assigned them to the treatment (Sindbis/FLuc) or vehicle (PBS) group. A combined and single xenograft-bearing model was chosen for a better differentiation of SINV targeting of different tumor entities

(combined model), but also to exclude/observe possible intertumoral interaction and its potential influence on viral infection rate (single model). Daily i.v. injections of Sindbis/FLuc (0.2 ml of Opti-MEM containing 10^6–10^7 CFU) were initiated on day 6. The bioluminescence signals were monitored using the IVIS system 200 (Caliper Life Sciences, Hopkinton, MA, USA) on day 6 (baseline, prior Sindbis/FLuc injection), days 8 and 10. Before imaging, each mouse was intra-peritoneally injected with 0.3 mL of luciferin (15 mg/mL potassium salt) in PBS. After 5 min, the mice were anesthetized with isoflurane/O_2. An integration time of 30 s was used for high-resolution luminescent imaging (binning: 2). The Living Image software (version 2.11; Caliper Life Sciences) was used to analyze the bioluminescence signals (total flux (photons/s)) from the animals.

Preparation of ^{18}F-FIAU/-FEAU

[^{18}F]-FIAU was synthesized as reported previously [17]. Briefly, [^{18}F]-fluoride was produced on cyclotron (EBCO TR 19/9, Richmond, British Columbia, Canada) using ^{18}O(p,n)^{18}F reaction. [^{18}F]-Fluoride (2.59–12.95 GBq) was trapped on Sep Pak QMA cartridge (Waters Corporation, Milford, MA, USA) and eluted into a 10-mL Reacti-vial using a solution containing 0.1 mL of potassium carbonate (0.25 M) and 0.9 mL of acetonitrile containing kryptofix (13.5 mg). Water was removed from the solution by azeotropic drying at 80 °C under a slow stream of argon. After initial drying, 1 mL of anhydrous acetonitrile was added and drying was repeated under the conditions above. The precursor 1,3,5-tri-O-benzoyl-2-trifluoromethylsulfonyl-α-D-ribofuranose (8–10 mg, ABX GMBH, Radeberg, Germany) was dissolved in anhydrous acetonitorle 300 μL and added to the anhydrous mixture of kryptofix, K_2CO_3 and [^{18}F]-KF in 10 mL glass vial and heated at 80 °C for 30 min. 2,4-*bis*(Trimethylsilyl)-5-iodouracil was synthesized by heating a solution of 5-iodouracil (10 mg), in dichloroethane (500 μL), hexamethyldisilizane (100 μL), and triemthylsilyltriflate (100 μL) in a sealed 3 mL V vial at 100 °C for 2 h. The radiolabeled sugar in 400 μL acetonitrile from the Advion unit was delivered directly to the vial containing 2,4-*bis* (trimethylsilyl)-5-iodouracil. The mixture was then heated at 85 °C for 60 min. The solvent was evaporated at 85 °C under stream of argon to yield a viscous oil. To this mixture, 0.5 M sodium methoxide in methanol (1 mL) was added and the reaction was heated at 85 °C for 5 min. The solvent was removed by heating at 85 °C under stream of argon and reconstituted in water (1 mL) and neutralized using 6 N HCl. The product was purified by using reverse-phase HPLC on a semipreparative C-18 column (Phenomenex, Luna, 250 × 10 mm 10 μm, C-18(2), 100 Å, Torrence, CA, USA) and using a mixture of 12 % acetonitrile and 88 % water containing acetic acid (0.2 %) at flow rate of 5 mL/min to yield a mixture of α- and β- anomers of [^{18}F]-FIAU. Solvent was removed on rotary evaporator and reconstituted in 0.9 % saline and passed through 0.22 μM filter for animal studies. [^{18}F]-FEAU was synthesized in a similar manner using 2,4-*bis*(trimethylsilyl)-5-ethyl uracil.

[^{124}I]-FIAU Uptake In Vitro

To determine the infectivity of the Sindbis/tk viral particles, 2×10^6 BHK, HT29, DU145, or HeLa cells were incubated with Sindbis/tk (MOI = 50) as described above. After washing and an overnight incubation period, the cells were exposed to 10 mL of culture medium containing 0.1 μCi of [^{124}I]-FIAU for 1, 2, 4, and 6 h. After each of these respective time

points, the radioactivity in the media and in the cell pellets was assayed in a liquid scintillation counter. Percentage uptakes of [^{124}I]-FIAU in cells were calculated as: (net counts in cell pellet)/(net counts in cell pellet+net counts in medium) × 100 %.

PET Studies

Xenograft mouse models of BHK and/or SK-MEL 10 or HT29 were prepared as described above and randomly assigned to untreated control (n = 3) and Sindbis/tk groups (n = 5). The Sindbis/tk group received i.v. injections consisting of 0.2 mL of Opti-MEM I containing 10^6–10^7 CFU of Sindbis/tk particles whereas control mice received 0.2 mL PBS. For PET imaging on day 3 (BHK/SK-MEL 10 and HT29) and day 6 (only HT29), mice were injected with about 0.3 mCi of [^{18}F]-FIAU (BHK/SK-MEL 10) or [^{18}F]-FEAU (HT29) via the tail vein. Two hours post-injection, the mice were anesthetized with isoflurane/O_2 and imaged on a R4 microPET™ (Concorde Microsystems, Knoxville, TN, USA), a dedicated 3D small-animal PET scanner. An energy window of 350–750 keV and a coincidence timing window of 6 ns were used, with a minimum of 20 million events, typically over 5 min, acquired. The resulting list-mode data was sorted into 2D histograms by Fourier rebinning and transverse images reconstructed by filtered back-projection into a 128 × 128 × 63 (0.72 × 0.72 × 1.3 mm) matrix. The reconstructed spatial resolution for ^{18}F is 1.5 mm full-width half maximum at the center of the field of view. The image data was corrected for non-uniformity of response of the microPET, deadtime count losses, and physical decay to the time of injection but no attenuation, scatter, or partial volume-averaging correction was applied. An empirically determined system calibration factor (millicuries per milliliter per counts per second per voxel) for mice was used to convert voxel count rates to activity concentrations and the resulting image data was then normalized to the administered activity to determine, by region of interest analysis, the maximum percentage injected dose per gram (%ID/g) in the tumors.

Fluorescence Molecular Tomography Measurements

BHK xenograft mice were i.v. injected with 2 nmol Angio-Sense™750 (150 mL volume, PerkinElmer, Waltham, MA, USA; excitation wavelength 750±10 nm, emission wavelength 780± 10 nm) and 300 μL of Sindbis/RC-FLuc solution or PBS on day 6 after tumor inoculation. To prevent fur interference with imaging, the tumor region of the skin was epilated. Fluorescence molecular tomography (FMT) imaging (FMT 2500, PerkinElmer, Waltham, MA, USA) was performed 24, 48, 72, and 96 h post-injection of the fluorophore; mice were anesthetized and placed in the imaging chamber one at a time. A near-infrared pair of laser diodes then scanned the region of interest (ROI) to provide multiple source-detector projections. In each ROI, we acquired 30 frontal slices of 0.5 mm thickness in z direction, with an in-plane resolution of 1× 1 mm. Laser excitation and fluorescence emission were detected by a single thermoelectrically cooled CCD camera with appropriate optical filters. The entire image acquisition sequence took ~2 min per mouse, followed by an automated dataset analysis using a normalized Born forward equation [18]. Three-dimensional ROIs were drawn around the tumor region and a threshold was applied equal to 10 % of the maximum value of fluorescence in each reconstructed volume to diminish quantification inaccuracies due to background signal and calibration variations [18, 19]. The

total amount (picomoles) of fluorochrome was automatically calculated relative to internal standards generated with known concentrations.

Results

Laminin Receptor Expression and Sindbis/FLuc Infection of Different Cancer Cell Lines

All human cancer cell lines used in these experiments clearly expressed the LR, using a polyclonal rabbit antibody to detect the 37 kDa laminin receptor precursor (Fig. 1a). Although not fully characterized, it is postulated that the mature 67 kDa LR is a homo- or heterodimer of its 37 kDa precursor [20]. The precursor is believed to be modified by fatty acid acylation in the maturation process and multiple studies have shown that the expression pattern of the LR precursor positively correlates with the mature 67 kDa form [21]. Evaluating the intensity of the luminescent signal using the IVIS 200 system as an indicator for the SINV infection rate (Fig. 1b), we saw a significant difference between the cell lines. BHK cells showed the strongest signal, indicating high cellular SINV load. Concomitantly, immunoblotting revealed BHK cells had the highest LR expression. In comparison, SK-MEL 10 produced about 50-fold lower bioluminescent signal and a clearly lower LR density. In terms of the other cell lines, however, no clear correlation of the LR expression pattern and the SINV infection rate could be determined, e.g., DU145 and H1650 cells clearly expressed LR, but showed basically no SINV uptake.

Sindbis/tk Infection of Different Cancer Cell Lines

Similar results could be observed using a Sindbis vector that mediates the synthesis of herpes simplex virus thymidine kinase type 1 (Sindbis/tk). After incubation with Sindbis/tk particles, the human cancer cell lines were exposed to [^{124}I]-FIAU, a thymidine kinase substrate. Significant intracellular tracer accumulation could be observed for the BHK cells (Fig. 2). SK-MEL 10 and HT29 also showed a clear radioactive signal, slightly increasing over time, but about 20–50 % lower than BHK cells. DU145 and HeLa cells only showed marginal detection levels of [^{124}I]-FIAU for the whole study period indicating very limited Sindbis/tk infection.

Sindbis/FLuc Infection In Vivo and Bioluminescence Imaging

To translate the *in vitro* to *in vivo* studies, a total of four daily virus injections were given to the tumor-bearing mice and IVIS imaging was performed on days 2 and 4 after initiation of viral application. A luminescent signal could, again, only be detected in the BHK tumors. Although the SK-MEL 10 xenografts were significantly smaller (in the combined and single xenograft model), increasing the time of imaging did not lead to any detectable signal that exceeded the background (Fig. 3). *In vivo* infection of Sindbis/FLuc particles seemed to clearly differ between the two tumor entities used in this setting.

Sindbis/tk Infection In Vivo and PET Imaging

Similar results could be obtained, treating the BHK/SK-MEL 10 or HT29 xenograft mice with Sindbis particles carrying the HSV 1-thymidine kinase gene and ^{18}F-FEAU PET imaging. The same time course as for optical imaging was chosen, including Sindbis/tk injections on four consecutive days, with PET performed after two and four viral

applications. Again, BHK xenografts showed a distinct tumoral thymidine kinase activity (1.7 %ID/g; Fig. 4c), whereas in SK-MEL 10 tumors the tracer uptake was limited (0.9 %ID/g; Fig. 4b, c), not reaching statistical significance as compared with vehicle-treated animals ($p = 0.08$; Fig. 4a, d). In BHK tumor mice, FEAU accumulation in the treated tumors, however, was significantly higher than in the control group ($p = 0.003$; Fig. 4d). Again, the BHK xenografts revealed a much more aggressive phenotype, resulting in much larger tumors compared to the melanomas.

HT29 tumors showed hardly any FEAU tracer uptake. Although the tumors could be differentiated from background activity, the mean uptake values (shown on days 2 and 4) in the treatment vs. nontreatment group were basically identical (Fig. 5).

Replication-Competent Sindbis/tk Infection In Vivo and Optical Imaging

We further wanted to evaluate the imaging feasibility of a replication-competent Sindbis vector carrying the FLuc gene (RC-FLuc) using FMT. We were interested to confirm virus replication in the tumors after single-dose injection by using bioluminescence imaging and, as SINV is a blood-born virus, to evaluate its delivery and tumoral distribution pattern using a vascular agent and FMT. As we observed the best *in vivo* infection rates with the BHK xenografts, we chose this model. Five mice were injected with a single dose of Sindbis RC-FLuc on day 0 while another three mice received just the PBS vehicle. Bioluminescence imaging was performed with the IVIS 200 system on four consecutive days. To study tumor vasculature, we used Angio- Sense™750, a fluorescence agent that enables visualization of tumor vascularity, perfusion, and vascular permeability. Each mouse was also injected with a single dose of this fluorescent agent on day 0 and quantitative imaging on the FMT 2500™ was performed. Looking at the signals obtained from the fluorophore and luciferin, a similar, although sometimes due to animal positioning misaligned, distribution pattern of both signals in the tumors could be observed (Fig. 6a and b). Within the first 24 h, AngioSense showed a predominantly central accumulation in the tumors, followed by a subsequent distribution to the tumor periphery. Semiquantitative analysis of the tumoral virus load showed a constant amplification within the first 3 days, indicating that SINV clearly infects the tumors in the first 24 h and replicates for about 72 h (Fig. 6b and 7). That virus delivery and distribution is dependent on tumor vascularisation could be underscored by the FMT data. AngioSense has a circulation half-life of about 6 h and undergoes subsequent renal excretion. As we observed, a cumulative enrichment of the fluorophore in the central tumor region within the first 24 h (not shown) and a constant signal for the following 2 days in the periphery, a transfer of the fluorescent agent from the vascular space to the interstitium seems to occur, followed by degradation of the dye after 3 days (Fig. 6a and 7). An almost identical dynamic of the bioluminescence and fluorescence signals emphasized the close relationship of tumor vascularization and tumoral virus distribution (Fig. 7).

Discussion

Alphavirus expression vectors have been employed to produce recombinant proteins in mammalian cells [22, 23]. SINV is a single-stranded, positive sense RNA virus, belonging

to the alphavirus family, that can infect a broad range of cells and replicate to high titres [24, 25]. It is transmitted by mosquitoes primarily to birds, but can cause fever, arthritis, and skin rash in humans [26]. SINV infection of mammalian cells is known to be mediated by the high-affinity 67 kDa LR [3], which has increased expression in many types of human cancers [4–7]. LR is known to play an important role in normal and tumor cell proliferation, protein translation, and survival. It is also involved in malignant cell metastasis by adherence to the basement membrane of other cells for subsequent infiltration and tumor spreading. [27–29].

The aim of our study was to evaluate the cellular infection rates of different, genetically modified SINV vectors in various tumor models and to review molecular imaging modalities, such as bioluminescence, FMT, and PET, for their feasibility to detect intratumoral viral load.

Although all the human cancer cell lines we used in our studies showed a marked expression of LR, the infection rates of the SINV particles differed significantly among the cell lines. Others have postulated that the SINV does not exclusively use the LR to infect its target cells. As the virus mainly seems to use heparan sulfate (HS) residues of the laminin receptor, it also interacts with nonreceptor-associated HS on the cell surface to enter the host cells [21, 30]. The HS binding region of the SINV mainly consists of the E2 glycoprotein, one of the viral envelope proteins and its interaction is mediated via two HS-binding domains. Alterations in the amino acid sequence of these domains result in changes of its electrostatic characteristics and may significantly decrease viral binding affinities and infection rates. Loss of HS affinity by the virus, however, does not necessarily have to result in loss of cellular targeting. A HS-independent way of viral infection which is not completely characterized has also been described, underlining the complex mechanisms SINV are able to obtain to reach their designated goal [31, 32]. It is unlikely that the different infections rates in our study are due to different binding site characteristics of the modified virus particles, as the basis for each modification was the same virus strain. It is also unlikely that the modifications we performed altered SINV infectivity, as we got good infection rates with each particle in the BHK cells. Presumably, the cells we tested differ significantly in non-LR-associated HS expression on the cell surface. A possible way to examine this hypothesis could be to co-incubate each cell line with the virus and an antibody against LR and see to what extent SINV infection can be blocked. In this context, others observed that using a monoclonal LR-Ab resulted in partial block of SINV infection, whereas in some cell lines viral infection could hardly be altered by blocking the receptor [3]. In this context, one also has to consider that, so far, the reliable working antibodies available mainly target the cytosolic form of LR. Thus, expression levels of the 37 kD LR might not be a good predictor of extracellular receptor expression. Further studies need to evaluate the role of LR in SINV infection in nonpermeabilized cells by, e.g., using binding assays. Also, one should consider fractionating the plasma membrane and quantifying LR expression solely in this cellular proportion.

A recent publication reports on an infection resistance of prostate and breast cancer cells in contrast to a good SINV infection of colorectal carcinoma cells [33]. All cell lines revealed a comparable expression of LR, but SINV susceptibility seemed to be mainly influenced by

the metastatic potentials of the cells. The more aggressive and invasive the cell line, the more effective SINV targeting *in vitro* and *in vivo*. The authors concluded that the viral infection rate is basically independent of cellular LR expression and suggest that a novel way of cell attachment or entry mechanism is employed by the virus during infection, resulting in preferred targeting of the more aggressive cellular phenotypes.

It has been shown that tumoral SINV infection modulates the immune system resulting in activation of cytotoxic natural killer (NK) cells and induction of anti-cancer M1 macrophages [34]. In an SINV-mediated encephalitis mouse model, NK cells proofed to have a significant effect on early viral clearance mediated by interferon (IFN)-γ and TNFα initiated and controlled T cell response [35]. On the other hand, it has been described that the mammalian innate immune system senses viral infection by recognizing viral signatures, mainly nucleotides, and activates potent antiviral responses and effects intracellular viral replication [36]. Besides the IFN response, RNA silencing or RNA interference (RNAi) serve as an antiviral mechanism in mammalian cells. To oppose this, some viruses are capable of encoding IFN antagonists, which counteract the IFN response in infected cells [37]. In addition, a number of viral IFN antagonists are capable of blocking RNAi in infected cells and therefore serve as RNA-silencing suppressors (RSS). Virus replication in infected cells can be restricted by these innate antiviral mechanisms, yielding in a suboptimal viral gene delivery [38]. Efficient blocking of the innate antiviral responses can be achieved by pretransfection of the host cells with a RSS, leading to an increase in viral vector production (up to 100-fold in terms of SINV) [37]. Further studies are needed to evaluate whether different pathways or activity levels of the innate antiviral response account for the observed diversity in infection rates of the human tumor cells used in our experiments.

Another aspect in antiviral immunity has been recently published, describing a protective role of cellular autophagy in antiviral response [39]. Briefly, autophagy can function as a cell protection mechanism, in which the cells sequester their own cytosol via the formation of lipid bi-layered vesicles, the autophagosomes. These autophagosomes then fuse with lysosomes for subsequent cytosolic protein degradation and reprocessing for reutilization [40]. With autophagic “self-digestion” cells are able to overcome a, for example, period of nutrient starvation or other stressful situations. Autophagy also seems to function in antiviral immunity. A recent study showed that after hepatitis C infection, some cells can upregulate the adaptor protein p62, which interacts with the viral capsid and subsequently targets the virus to autophagosomes and lysosomal degradation [41]. A possible scenario is that this also accounts for SINV infection in some cells, meaning that the viral proteins might get cleared from the cell and the promotion of cell survival is obtained.

Viral vectors are a potentially powerful tool for delivering a therapeutic gene to tumors and metastatic disease. Systemic tumor targeting and tumor specificity would be ideal characteristics of these vectors to efficiently oppose neoplastic tissues while sparing the rest of the body. In this report, we used novel molecular imaging techniques to visualize vector delivery to different tumor entities. The tumor infection rates of SINV, however, were shown to differ among various cancer cell lines and did not seem to be dependent upon the cellular laminin receptor expression. The exact mechanism of SINV tumor targeting, needs

to be clarified in further studies. In terms of SINV vector delivery, we were able to confirm the correlation between tumor vascularisation, vascular leakiness and the tumoral virus distribution. Our results indicate that blood vessel permeability in tumors has a significant function in successful Sindbis virus vector targeting and tumoral tranduction [42].

Acknowledgments

We thank the staff of the Radiochemistry/Cyclotron Core at MSKCC. Technical services provided by the MSKCC Small-Animal Imaging Core Facility were supported in part by NIH grants R24 CA83084 and P30 CA08748. Technical services provided by the MSKCC Small- Animal Imaging Core Facility were supported in part by the NIH (R24 CA83084 and P30 CA08748). Lars Stelter was supported by the Deutsche Forschungsgemeinschaft (Ste 1837/1-1). Steven M. Larson was supported by the Ludwig Center for Cancer Immunotherapy at MSKCC and the National Cancer Institute (P50-CA86483).

References

1. Tseng JC, Levin B, Hirano T, Yee H, Pampeno C, Meruelo D. *In vivo* antitumor activity of sindbis viral vectors. J Natl Cancer Inst. 2002; 94:1790–1802. [PubMed: 12464651]
2. Tseng J, Levin B, Hurtado A, Yee H, Perez de Castro I, Jimenez M, et al. Systemic tumor targeting and killing by Sindbis viral vectors. Nat Biotechnol. 2004; 22:70–77. [PubMed: 14647305]
3. Wang K, Kuhn RJ, Strauss EG, Ou S, Strauss JH. High-affinity laminin receptor is a receptor for Sindbis virus in mammalian cells. J Virol. 1992; 66:4992–5001. [PubMed: 1385835]
4. Liebman JM, Burbelo PD, Yamada Y, Fridman R, Kleinman HK. Altered expression of basement-membrane components and collagenases in ascitic xenografts of OVCAR-3 ovarian cancer cells. Int J Cancer. 1993; 55:102–109. [PubMed: 8344742]
5. Ozaki I, Yamamoto K, Mizuta T, Kajihara S, Fukushima N, Setoguchi Y, et al. Differential expression of laminin receptors in human hepatocellular carcinoma. Gut. 1998; 43:837–842. [PubMed: 9824613]
6. Sanjuan X, Fernandez P, Miquel R, Munoz J, Castronovo V, Menard S, et al. Overexpression of the 67-kD laminin receptor correlates with tumour progression in human colorectal carcinoma. J Pathol. 1996; 179:376–380. [PubMed: 8869283]
7. van den Brule FA, Berchuck A, Bast R, Liu FT, Gillet C, Sobel ME, et al. Differential expression of the 67-kD laminin receptor and 31-kD human laminin-binding protein in human ovarian carcinomas. Eur J Cancer. 1994; 30A(8):1096–1099. [PubMed: 7654437]
8. Balachandran S, Roberts PC, Kipperman T, Bhalla KN, Compans RW, Archer DR, et al. Alpha/beta interferons potentiate virus-induced apoptosis through activation of the FADD/Caspase-8 death signaling pathway. J Virol. 2000; 74:513–1523. [PubMed: 10590141]
9. Levine B, Huang Q, Isaacs JT, Reed JC, Griffin DE, Hardwick JM. Conversion of lytic to persistent alphavirus infection by the bcl-2 cellular oncogene. Nature. 1993; 361:739–742. [PubMed: 8441470]
10. Zrachia A, Dobroslav M, Blass M, Kazimirsky G, Kronfeld I, Blumberg PM, et al. Infection of glioma cells with Sindbis virus induces selective activation and tyrosine phosphorylation of protein kinase C delta. Implications for Sindbis virus-induced apoptosis. J Biol Chem. 2002; 277:23693–23701. [PubMed: 11927579]
11. Caruso M, Panis Y, Gagandeep S, Houssin D, Salzmann JL, Klatzmann D. Regression of established macroscopic liver metastases after in situ transduction of a suicide gene. Proc Natl Acad Sci U S A. 1993; 90:7024–7028. [PubMed: 8346212]
12. Mar EC, Chiou JF, Cheng YC, Huang ES. Human cytomegalovirus-induced DNA polymerase and its interaction with the triphosphates of 1-(2′-deoxy-2′-fluoro-beta-D-arabinofuranosyl)-5-methyluracil,-5-iodocytosine, and-5-methylcytosine. J Virol. 1985; 56:846–851. [PubMed: 2999440]
13. Beltinger C, Fulda S, Kammertoens T, Uckert W, Debatin KM. Mitochondrial amplification of death signals determines thymidine kinase/ganciclovir-triggered activation of apoptosis. Cancer Res. 2000; 60:3212– 3217. [PubMed: 10866313]

14. Beltinger C, Fulda S, Kammertoens T, Meyer E, Uckert W, Debatin KM. Herpes simplex virus thymidine kinase/ganciclovir-induced apoptosis involves ligand-independent death receptor aggregation and activation of caspases. Proc Natl Acad Sci U S A. 1999; 96:8699–8704. [PubMed: 10411938]
15. Serganova I, Doubrovin M, Vider J, Ponomarev V, Soghomonyan S, Beresten T, et al. Molecular imaging of temporal dynamics and spatial heterogeneity of hypoxia-inducible factor-1 signal transduction activity in tumors in living mice. Cancer Res. 2004; 64:6101–6108. [PubMed: 15342393]
16. Tjuvajev JG, Finn R, Watanabe K, Joshi R, Oku T, Kennedy J, et al. Noninvasive imaging of herpes virus thymidine kinase gene transfer and expression: a potential method for monitoring clinical gene therapy. Cancer Res. 1996; 56:4087–4095. [PubMed: 8797571]
17. Anderson H, Pillarsetty N, Cantorias M, Lewis JS. Nucl Med Biol. 2010; 37:439–442. [PubMed: 20447555]
18. Ntziachristos V, Schellenberger EA, Ripoll J, et al. Visualization of antitumor treatment by means of fluorescence molecular tomography with an annexin V-Cy5.5 conjugate. PNAS. 2004; 101(33): 12294–12299. [PubMed: 15304657]
19. Ntziachristos V, Tung CH, Bremer C, et al. Fluorescence molecular tomography resolves protease activity *in vivo*. Nature Med. 2002; 8(7):757–760. [PubMed: 12091907]
20. Jamieson KV, Wu J, Hubbard SR, Meruelo D. Crystal structure of the human laminin receptor precursor. J Biol Chem. 2008; 6:3002–3005. [PubMed: 18063583]
21. Nelson J, McFerran NV, Pivato G, Chambers E, Doherty C, Steele D, et al. The 67kDa laminin receptor: structure, function and role in disease. Biosc Rep. 2008; 28:33–48.
22. Lundstrom K. Biology and application of alphaviruses in gene therapy. Gene Ther. 2005; 12:S92–S97. [PubMed: 16231060]
23. Nanda K, Vancini R, Ribeiro M, Brown DT, Hernandez R. A high capacity Alphavirus heterologous gene delivery system. Virology. 2009; 390:368–373. [PubMed: 19535122]
24. Tseng JC, Hurtado A, Yee H, Levin B, Boivin C, Benet M, et al. Using sindbis viral vectors for specific detection and suppression of advanced ovarian cancer in animal models. Cancer Res. 2004; 64:6684–6692. [PubMed: 15374985]
25. Tseng JC, Zanzonico PB, Levin B, Finn R, Larson SM, Meruelo D. Tumor-specific *in vivo* transfection with HSV-1 thymidine kinase gene using a Sindbis Viral vector as a basis for prodrug ganciclovir activation and PET. J Nucl Med. 2006; 47:1136–1143. [PubMed: 16818948]
26. Kurkela S, Manni T, Myllynen J, Vaheri A, Vapalahti O. Clinical and laboratory manifestations of sindbis virus infection: prospective study, Finland, 2002–2003. J Infect Dis. 2005; 191:1820–1829. [PubMed: 15871114]
27. Scheiman J, Tseng JC, Zheng Y, Meruelo D. Multiple functions of the 37/67-kd laminin receptor make it a suitable target for novel cancer gene therapy. Mol Ther. 2010; 18:63–74. [PubMed: 19724263]
28. Scheiman J, Jamieson KV, Ziello J, Tseng JC, Meruelo D. Extraribosomal functions associated with the C terminus of the 37/67kDa laminin receptor are acquired for maintaining cell viability. Cell Death Dis. 2010; 1:e42. [PubMed: 21243100]
29. Hand PH, Thor A, Schlom J, Rao CN, Liotta L. Expression of laminin receptor in normal and carcinomatous human tissues as defined by a monoclonal antibody. Cancer Res. 1985; 45:2713–2719. [PubMed: 3157447]
30. Ryman KD, Gardner CL, Burke CW, Meier KC, Thompson JM, Klimstra WB. Heparan sulfate binding can contribute to the neurovirulence of neuroadapted and nonneuroadapted sindbis viruses. J Virol. 2007; 81:3563–3573. [PubMed: 17215278]
31. Klimstra WB, Ryman KD, Johnston RE. Adaptation of Sindbis virus to BHK cells selects for use of heparan sulfate as an attachment receptor. J Virol. 1998; 72:7357–7366. [PubMed: 9696832]
32. Rowell JF, Griffin DE. The inflammatory response to nonfatal Sindbis virus infection of the nervous system is more severe in SJL than in BALB/c mice and is associated with low levels of IL-4 mRNA and high levels of IL-10-producing CD4+ T cells. J Immunol. 1999; 162:1624–1632. [PubMed: 9973422]

33. Bear JS, Byrnes AP, Griffin DE. Heparin-binding and patterns of virulence for two recombinant strains of Sindbis virus. Virology. 2001; 347:183–190. [PubMed: 16380143]

34. Granot T, Venticinque L, Tseng J-C, Meruelo D. Activation of cytotoxic and regulatory functions of NK cells by Sindbis viral vectors. PLoS One. 2010; 6:e20598. [PubMed: 21674047]

35. Li C, Gu Y, Andrade D, Liu Y. Susceptibility of colorectal cancer cells to Sindbis virus infection. J Exp Ther Oncol. 2009; 8:167–175. [PubMed: 20192123]

36. De Vries W, Haasnot J, van der Velden J, van Montfort T, Zorgdrager F, Paxton W, et al. Increased virus replication in mammalian cells by blocking intracellular innate defense responses. Gene Ther. 2008; 15:545–552. [PubMed: 18273055]

37. Hayman A, Comely S, Lackenby A, Murphy S, McCauley J, Goodbourn S, et al. Variation in the ability of human influenzy A viruses to induce and inhibit the IFN-β pathway. Virology. 2006; 347:52–64. [PubMed: 16378631]

38. Myles KM, Wiley MR, Morazzani EM, Adelman ZN. Alphavirus-derived small RNAs modulate pathogenesis in disease vector mosquitoes. Proc Natl Acad Sci U S A. 2008; 105:19938–19943. [PubMed: 19047642]

39. Orvedahl A, MacPherson S, Sumpter R, Talloczy Z, Zou Z, Levine B. Autophagy protects against Sindbis virus infection of the central nervous system. Cell Host Microbe. 2010; 7:115–127. [PubMed: 20159618]

40. Mizushima N, Levine B, Cuervo AM, Klionsky DJ. Autophagy fights disease through cellular self-digestion. Nature. 2008; 451:1069–1075. [PubMed: 18305538]

41. Ke PY, Chen SS. Activation of the unfolded protein response and autophagy after hepatitis C virus infection suppresses innate antiviral immunity in vitro. J Clin Invest. 2011; 121:37–56. [PubMed: 21135505]

42. Tseng JC, Granot T, DiGiacomo V, Levin B, Meruelo D. Enhanced specific delivery and targeting of oncolytic Sindbis viral vectors by modulating vascular leakiness in tumor. Cancer Gene Ther. 2010; 17:244–255. [PubMed: 19798121]

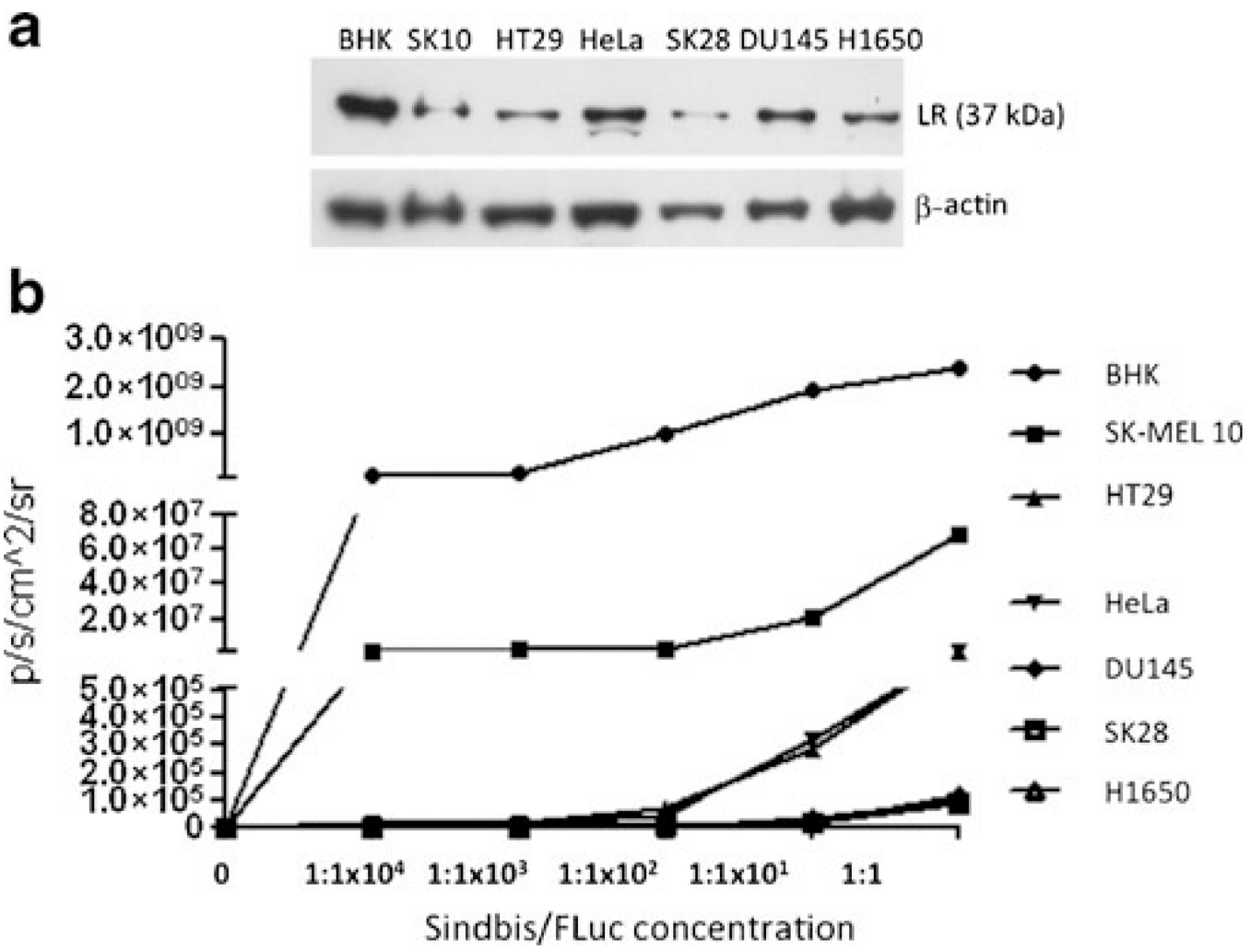

Fig. 1.

a Western Blot analysis of cancer cell lines indicating laminin receptor (LR) expression. **b** Bioluminescence signal of cells incubated with Sindbis/FLuc particles at different concentrations.

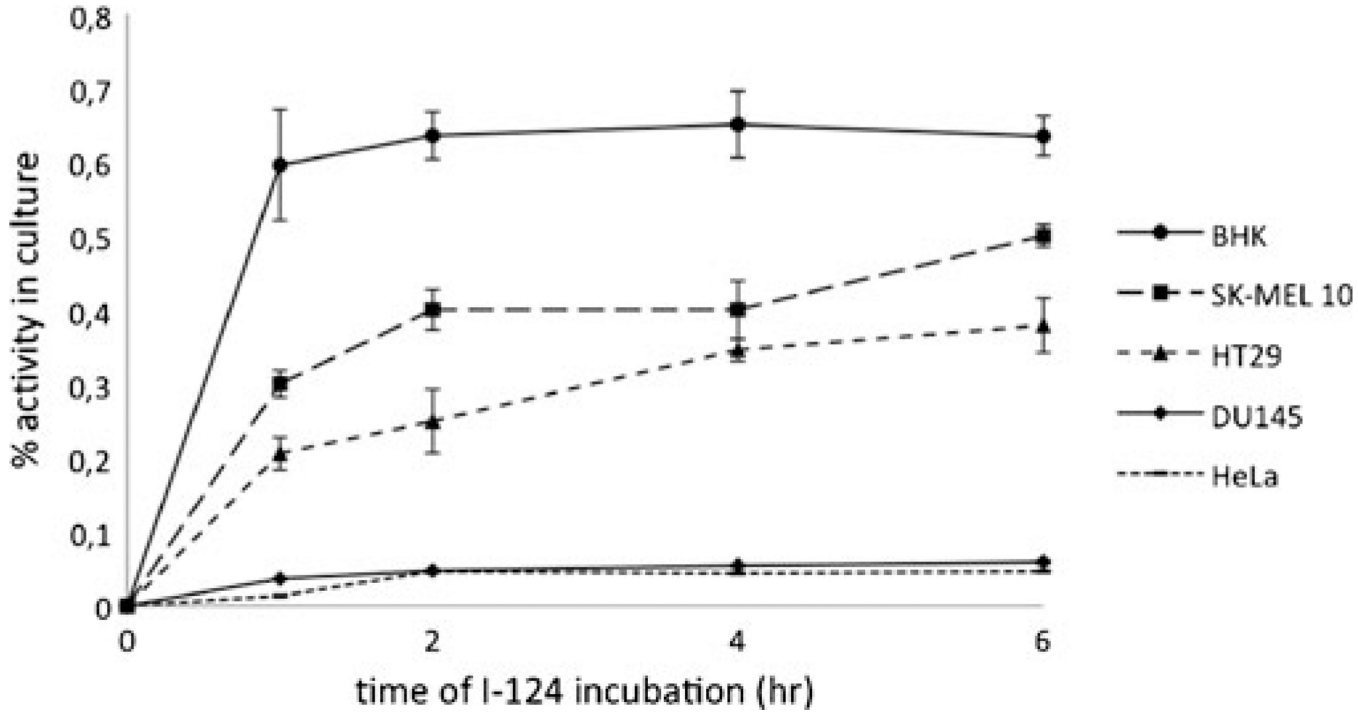

Fig. 2.

Intracellular accumulation of ^{124}I-FIAU after infection of different human cancer cell lines with Sindbis/tk particles.

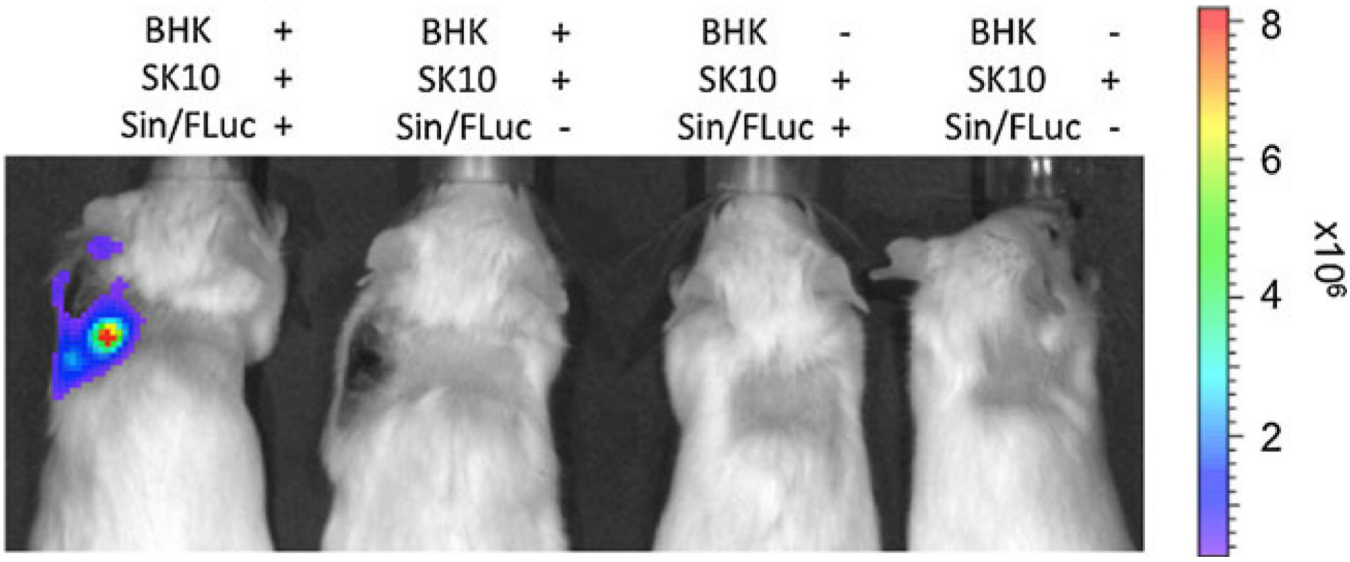

Fig. 3.

Bioluminescence imaging of mice bearing BHK and/or SK-MEL 10 xenografts after i.v. application of Sindbis/FLuc particles.

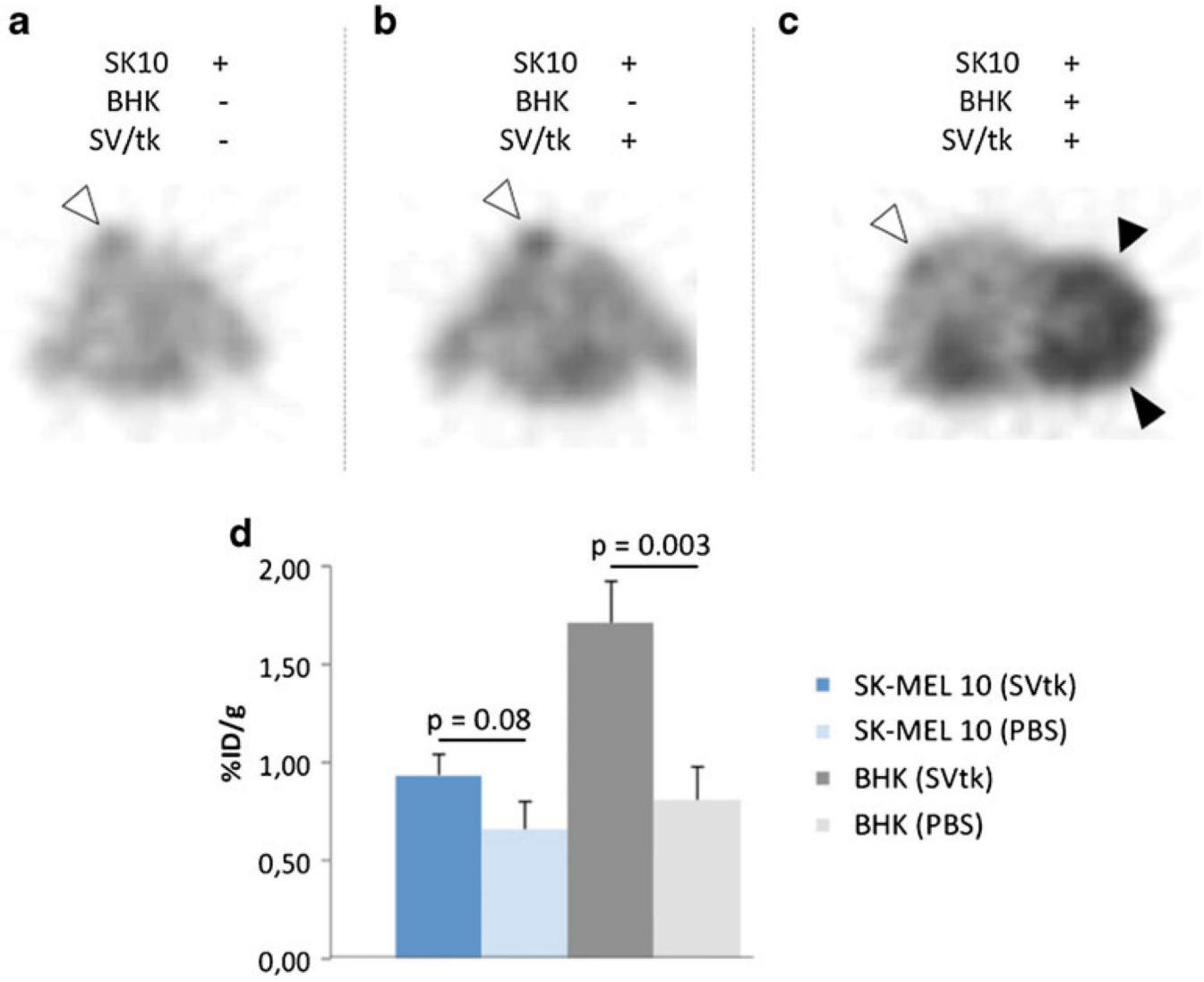

Fig. 4.

^{18}F-FEAU PET of BHK and SK-MEL 10 tumor-bearing mice after injection with Sindbis/tk particles (SV/tk) (**b, c**) and vehicle treated mice (**a**). Tumoral tracer quantification using ROI analysis is shown in (**d**).

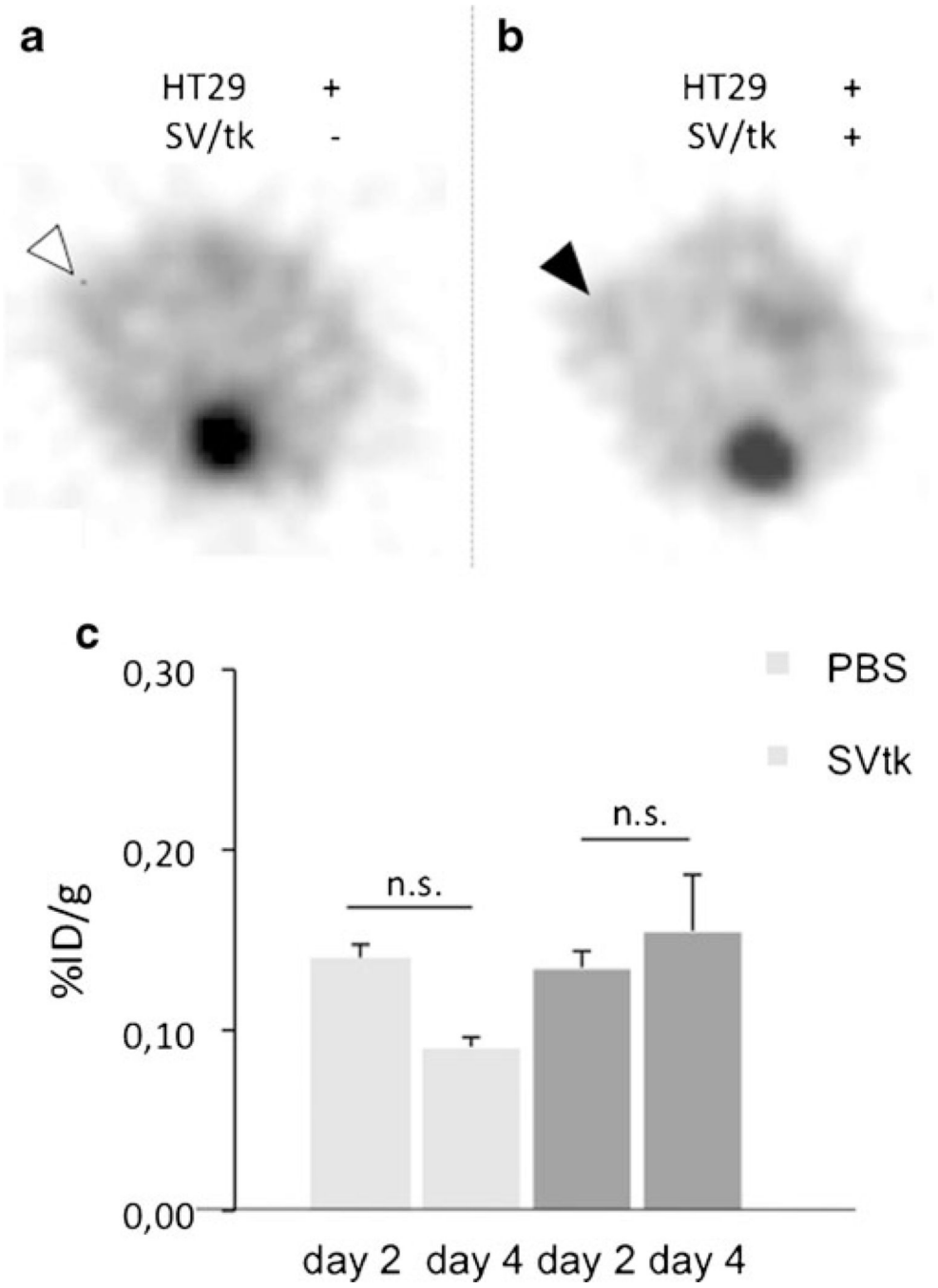

Fig. 5.

^{18}F-FEAU PET of HT29 tumor-bearing mice after injection with Sindbis/tk particles (SV/tk) (**b**) and vehicle treated mice (**a**). Tumoral tracer quantification using ROI analysis is shown in (**c**).

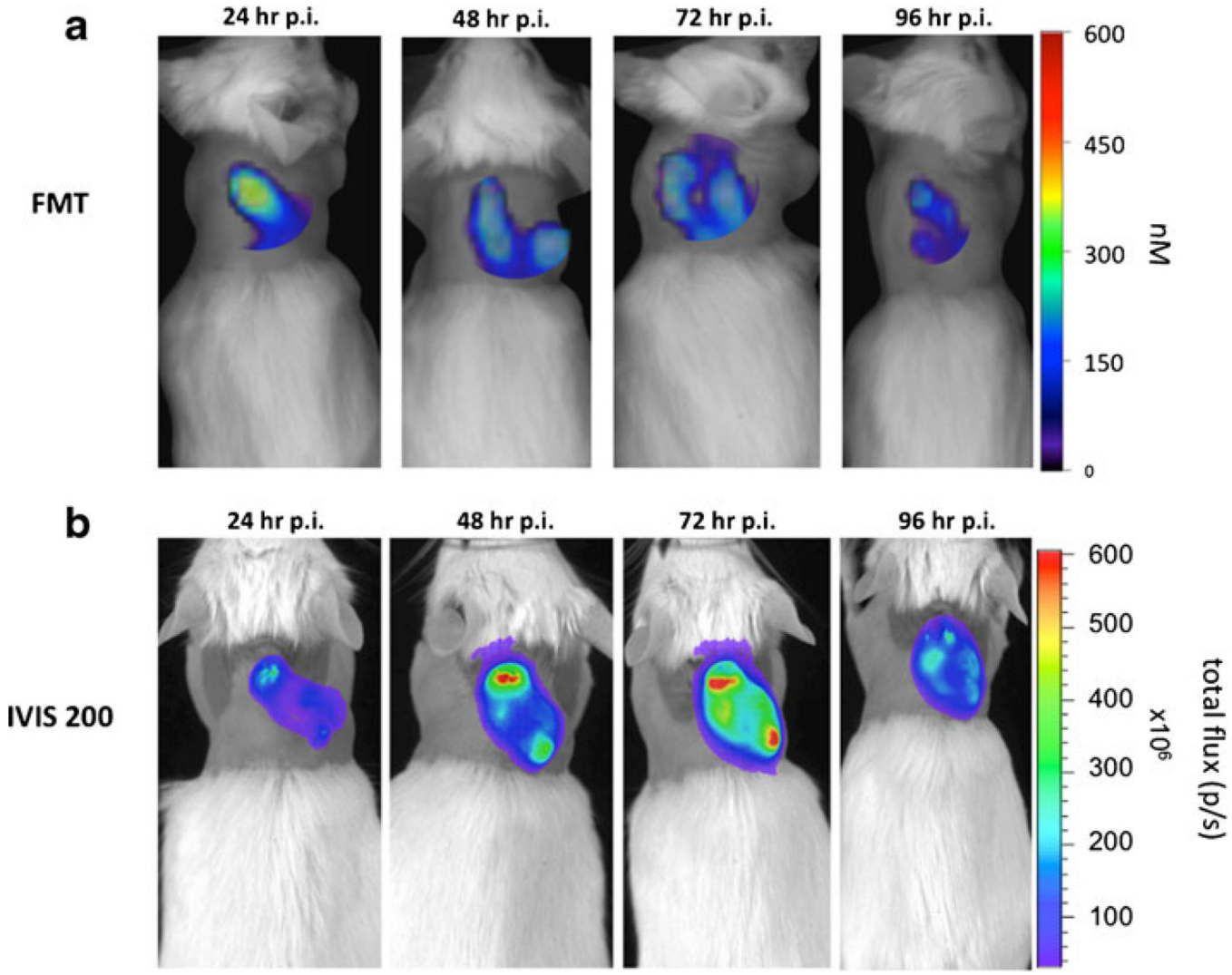

Fig. 6.

AngioSense™750 in FMT a and bioluminescence imaging (IVIS 200) b after injection of a replication-competent SINV vector carrying the FLuc gene.

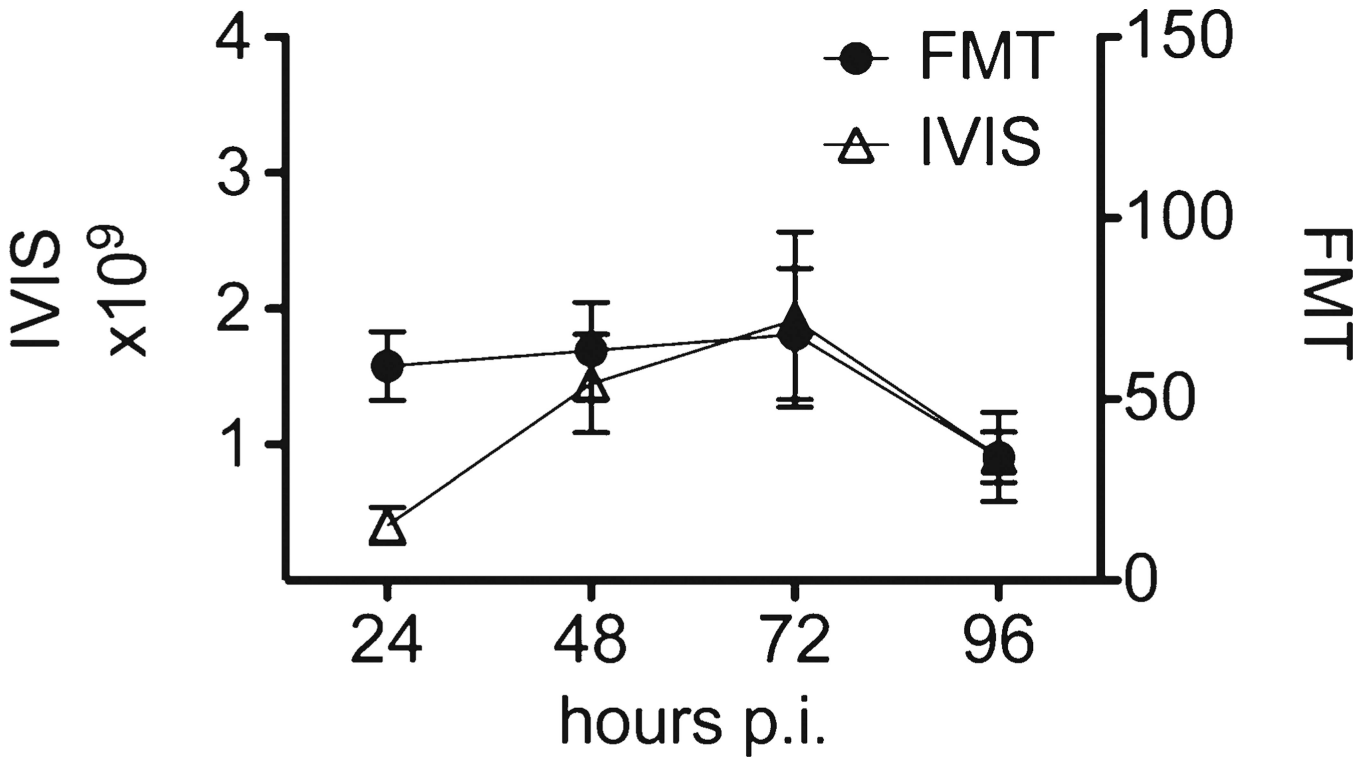

Fig. 7.
ROI analysis of the FMT and IVIS data (Fig. 6).